How well can satellite data characterize the water cycle of the Madden-Julian Oscillation?

Duane E. Waliser,[1] Baijun Tian,[1,2] Xiaosu Xie,[1] W. Timothy Liu,[1] Michael J. Schwartz,[1] and Eric J. Fetzer[1]

Received 9 July 2009; revised 15 September 2009; accepted 24 September 2009; published 6 November 2009.

[1] Most characterizations of the Madden-Julian Oscillation (MJO) have focused on its convection and circulation features, ocean interactions, and weather and climate impacts. The water cycle of the MJO has yet to be examined or quantified despite it offering an additional constraint on model representations of the MJO, which are still woefully poor. Recent satellite products now make it possible to characterize the MJO water cycle from observations. These include water vapor profiles, column water vapor, cloud ice profiles, total cloud liquid, rainfall, surface evaporation and column moisture convergence. From these, we quantify the water budget for disturbed and suppressed phases of the MJO. The column-integrated results indicate that precipitation is nearly balanced with moisture convergence, with variations in surface evaporation being an order of magnitude smaller. However, residuals in the column-integrated budget are relatively large, indicating the need for improved satellite retrievals and/or the necessity of using model-based assimilation products.
Citation: Waliser, D. E., B. Tian, X. Xie, W. T. Liu, M. J. Schwartz, and E. J. Fetzer (2009), How well can satellite data characterize the water cycle of the Madden-Julian Oscillation?, *Geophys. Res. Lett.*, *36*, L21803, doi:10.1029/2009GL040005.

1. Introduction

[2] The most notable form of subseasonal variability in the Tropics is the Madden-Julian Oscillation (MJO) [*Madden and Julian*, 1971; *Lau and Waliser*, 2005; *Zhang*, 2005]. Interest in tropical intraseasonal (30–90 day) variability has intensified in recent years [*Sperber and Waliser*, 2008] due to the promise it holds for providing an element of predictability in the gap between time scales of weather and seasonal variability. There has been considerable effort characterizing the MJO's circulation features and their connections to rainfall and clouds, as well as its interactions with near-surface heat and momentum fluxes [*Weickmann et al.*, 1992; *Hendon and Salby*, 1994; *Waliser et al.*, 2003]. To a great degree, the objective of these studies has been to derive a better understanding of the MJO and its impacts through the characterization of the connections between the dynamical and thermodynamic features of the MJO. More recently there has also been efforts to characterize and understand the manner the MJO interacts with the biochemical aspects of the Earth system [*Waliser et al.*, 2005; *Tian et al.*, 2007, 2008].

[3] Despite the above wealth of studies on the MJO, there have been few comprehensive studies that characterize the energy and water cycles associated with the MJO. Some components of these cycles have been addressed in studies focused on for example the surface energy budget, rainfall and water vapor variations, and cloud and radiation relationships [e.g., *Lau and Sui*, 1997; *Lin et al.*, 2004; *Mu and Zhang*, 2006]. A major limitation in conducting more comprehensive studies has been the lack of a complete set of observations. This has been overcome in a few instances to study the energetics of the MJO either by virtue of a field program (i.e., TOGA COARE) [e.g., *Lin and Johnson*, 1996; *Lin and Mapes*, 2004] or by using a modeling framework [e.g., *Mu and Zhang*, 2006]. To the best of our knowledge, there has been no comprehensive examination of the hydrological cycle of the MJO, particularly not on a global scale. In this study, we utilize a number of contemporary satellite data sets to characterize the atmospheric hydrological cycle of the MJO.

2. Observations

[4] For atmospheric water vapor profiles, we use the Atmospheric Infra-red Sounder (AIRS) Level 3 V.4 products from the combined AIRS and atmospheric microwave sounding unit (AMSU) retrievals [*Chahine et al.*, 2006; *Susskind et al.*, 2006]. Total column water vapor data are from AIRS (1° × 1°; 9/1/02–4/30/07; twice-daily) as well as from the F13 Special Sensor Microwave Imager (SSM/I; 0.25° × 0.25°; 1/1/96–6/30/07; twice-daily) [*Wentz*, 1997]. The rainfall data are from both the CPC merged analysis of precipitation (CMAP; 2.5° × 2.5°; 1/1/79–2/22/07; 5-day) [*Xie and Arkin*, 1997; *Xie et al.*, 2003] and the Tropical Rainfall Measurement Mission (TRMM; 0.25° × 0.25°; 1/1/98–6/30/07; 5-day) 3B42 product [*Huffman et al.*, 2007]. The availability of two data sources for water vapor and precipitation provides the ability to illustrate a measure of observational uncertainty. The total column liquid water is from SSM/I [*Wentz and Spencer*, 1998] (0.25° × 0.25°; 1/1/96–6/30/07; twice-daily). The cloud ice water content (IWC) is from the Microwave Limb Sounder (MLS; 4° × 8°; 8/26/04–2/22/07; daily) [*Wu et al.*, 2006]. MLS provides an estimate of IWC for the upper troposphere, namely for pressure levels less than about 300 hPa. Discussions and applications of the use of this data set are given by *Wu et al.* [2009] and *Waliser et al.* [2009]. The moisture transport integrated over the depth of the atmosphere (0.5° × 0.5°; 9/1/99–12/31/2005; twice-daily) is estimated by *Xie et al.* [2008] [see also *Liu and Tang*, 2005] using the surface wind

[1] Jet Propulsion Laboratory, California Institute of Technology, Pasadena, California, USA.
[2] Joint Institute for Regional Earth System Science and Engineering, University of California, Los Angeles, California, USA.

0094-8276/09/2009GL040005

vector from Quick Scatterometer (QuikSCAT), cloud-drift wind vector from the Multi-angle Imaging Spectroradiometer (MISR) and NOAA geostationary satellites, and the precipitable water from the SSM/I. The total column moisture convergence (TCMC) is then calculated from the total-column moisture transport [with convergence (divergence) of moisture defined to be >0 (<0)]. The surface evaporation is based on the oceanic latent heat flux product generated by the OAFlux project [*Yu and Weller*, 2007] (1° × 1°; 1/1/81–12/31/02; daily). These retrievals are derived from a synthesis of satellite observations from SSM/I, QuikSCAT, Advanced Very High Resolution Radiometer (AVHRR), TMI, and Advanced Microwave Scanning Radiometer Earth Observing System (EOS) (AMSR-E) and numerical weather model outputs (e.g., ECMWF operational forecast analysis, ERA-40 and NCEP reanalyses) using a variational objective analysis technique.

[5] For the MJO analysis procedure, we use the compositing approach from our previous papers [e.g., *Waliser et al.*, 2003; *Tian et al.*, 2006]. Briefly, all the data were first binned into pentad values and then intraseasonal anomalies of the data were obtained by removing the annual cycle and filtering via a 30–90-day band pass filter. To isolate the dominant structure of the MJO, an extended empirical orthogonal function (EEOF) [*Weare and Nasstrom*, 1982] analysis was applied using time lags of ±5 pentads (i.e., 11 pentads total) on boreal winter (November–April) rainfall for the region 30°S–30°N and 30°E–150°W (Figure S1 of the auxiliary material).[1] Next, MJO events were chosen based on the amplitude (>1) time series of the first EEOF mode of the rainfall anomaly. Figure S1 shows the dates and number of the selected MJO events for each data set. For each selected MJO event, the corresponding 11-pentad period for each data set were extracted. A composite was obtained by averaging the selected MJO events. In Figure S1, we plot lags −2, 0, +2 and +4; note that lag −4 is very similar to lag +4 which indicates about a 40 day cycle.

3. Results

[6] Figure 1 illustrates some measures of observational uncertainty for those quantities in which more than one satellite product is available. Figure 1a shows the composite precipitation patterns from both CMAP (contour) and TRMM (shading). Evident is the rather good agreement (correlation over all lags and grid points is 0.88), even extending to some of the isolated small anomalies remote from the tropical Indian and western Pacific Ocean. To show the level agreement more quantitatively, the upper right panel shows the meridional-average precipitation using the CMAP record (purple), the TRMM record (black), and the CMAP data for the TRMM period (green). The overall agreement is quite good, with each exhibiting anomalies up to about ±3 mm day^{-1}. The correlation for the meridional composite rainfall when using the entire CMAP and entire TRMM record is 0.90, when using the shorter TRMM period (i.e., 1998–07) only for each data set is 0.95, and for the CMAP data alone using the entire length and only the data from the TRMM period is 0.95. The RMS difference between any two of the meridional-average precipitation composites is about 0.03 mm day^{-1} (not shown). Similar information is provided for the total column water vapor in the lower left panel using the AIRS and SSMI estimates. In this case, the anomalies are on the order ±2 mm, and RMS differences are about 0.2 mm (not shown). The correlation for the near-equatorial meridional-average of the composite water vapor when using the entire SSMI and entire AIRS record is 0.87, when using the AIRS period (i.e., 2002–07) only is 0.95, and for the SSMI record using the entire length and only the AIRS period is 0.90. Both sets of line plots and their correlations indicate close agreement when the two data sets are sampled over the same events/period, with greater sensitivity to the differences in period over which the MJO events are selected rather than the choice of the data set used – at least for the variables and data sets shown here.

[7] Figure 2 shows the composite structures of precipitation (contours in each map), column TCMC (Figure 2, top left), evaporation (Figure 2, bottom left), column water vapor (Figure 2, top right) and column cloud liquid water (Figure 2, bottom right) in terms of latitude-longitude maps. In each case, the precipitation is sampled using the same events available for the quantity that is plotted in color shading (Figure S1). Comparison of these four line contour maps further illustrates the degree the composite MJO depends on the time period, and thus the events, sampled. Generally speaking, TCMC is in phase with positive rainfall anomalies, and with a similar magnitude, with a correlation of 0.5. Composite average column water vapor anomalies are on the order of ±2 mm, with a correlation to rainfall of 0.42. They also tend to be in phase with precipitation although the spatial correspondence is less clear and there is some hint that the moisture may be leading the precipitation in some phases (see Figure 3, top right). The lead-lag relationships between these three quantities, along with their implications on the theoretical understanding of the MJO, are more rigorously examined by (B. Tian et al., On the low-level moisture preconditioning of the Madden-Julian Oscillation, submitted to *Journal of Climate*, 2009).

[8] In the near-equatorial region, the evaporation anomalies are about a factor of 10 smaller than the precipitation and TCMC anomalies. The largest of the evaporation anomalies lie between about 15–30° latitudes and occur in the northwest and north central Pacific Ocean. In the 0 (+4) lag pentad composite, there are low-level anti-cyclonic (cyclonic) wind structures that develops in association with the Rossby wave component, the centers of which lie at about 20° latitude and 170°E [*Hendon and Salby*, 1994]. The west (east) side of this anti-cyclonic pattern results in poleward (equatorward) winds occurring in conjunction with the large negative (positive) evaporation anomalies, suggesting that the transport of warm, moist (cold, dry) air may play an important role in producing these anomalies. There is a very close correspondence between the cloud liquid water anomalies and the precipitation anomalies (correlation is 0.89), with the former ranging up to ±0.02 mm for the composite average MJO.

[9] Figure 3 (top) illustrates the vertical structure of the water vapor anomalies though the troposphere and the cloud ice anomalies in the upper troposphere/lower stratosphere. The former were illustrated and discussed in detail by *Tian*

[1] Auxiliary materials are available in the HTML. doi:10.1029/2009GL040005.

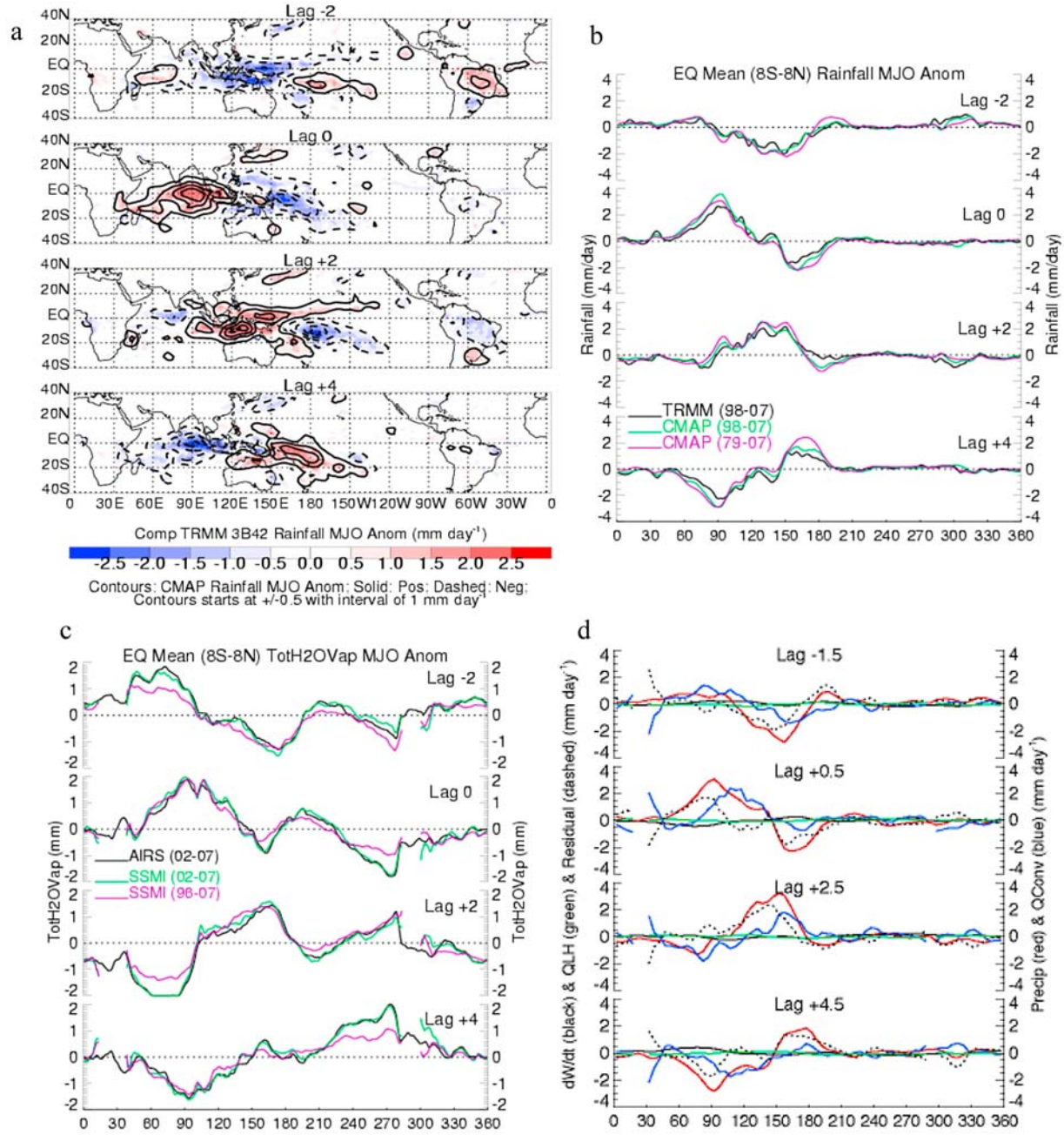

Figure 1. (a) Maps of composite TRMM and CMAP rainfall anomalies (mm day^{-1}) for the TRMM period (1998–2007). (b) Composite near-equatorial (8°S–8°N) rainfall anomaly (mm day^{-1}) for TRMM from 1998 to 2007 and CMAP from 1998 to 2007 and from 1979 to 2007. (c) Composite near-equatorial (8°S–8°N) precipitable water anomaly (mm) for AIRS from 2002 to 2007 and SSMI from 2002 to 2007 and from 1996 to 2007. (d) Composite near-equatorial (8°S to 8°N) anomalies of total water vapor storage (black), rainfall (red), moisture convergence (blue), surface evaporation (green), and their residuals (dashed) (mm day^{-1}).

et al. [2006] and the latter by *Schwartz et al.* [2008]. Also shown in Figure 3 (top) are the near-equatorial averages of precipitation, TCMC and evaporation on the left, and precipitation, total column water vapor and total column liquid water on the right. Evident is the tilted structure of the water vapor anomalies (westward with height) in the Indian and west Pacific Ocean regions, with low-level moisture preceding the positive precipitation anomalies; additional discussion by (Tian et al., submitted manuscript, 2009). For cloud ice, the precipitation and liquid water content anomalies are well correlated, except in the eastern Pacific at lag 0 where the cloud ice anomalies are relatively large but the precipitation anomalies are relatively small. Note also that the cloud ice anomalies reach pressure levels about 50 hPa lower over the Indo-Pacific region, where the precipitation anomalies and the mean rising motion is largest, compared to the anomalies occurring over Africa, S. America and the eastern Pacific. Notable are the sizeable water vapor anomalies in the eastern Pacific that occur in conjunction with what appear to be near-zero precipitation anomalies.

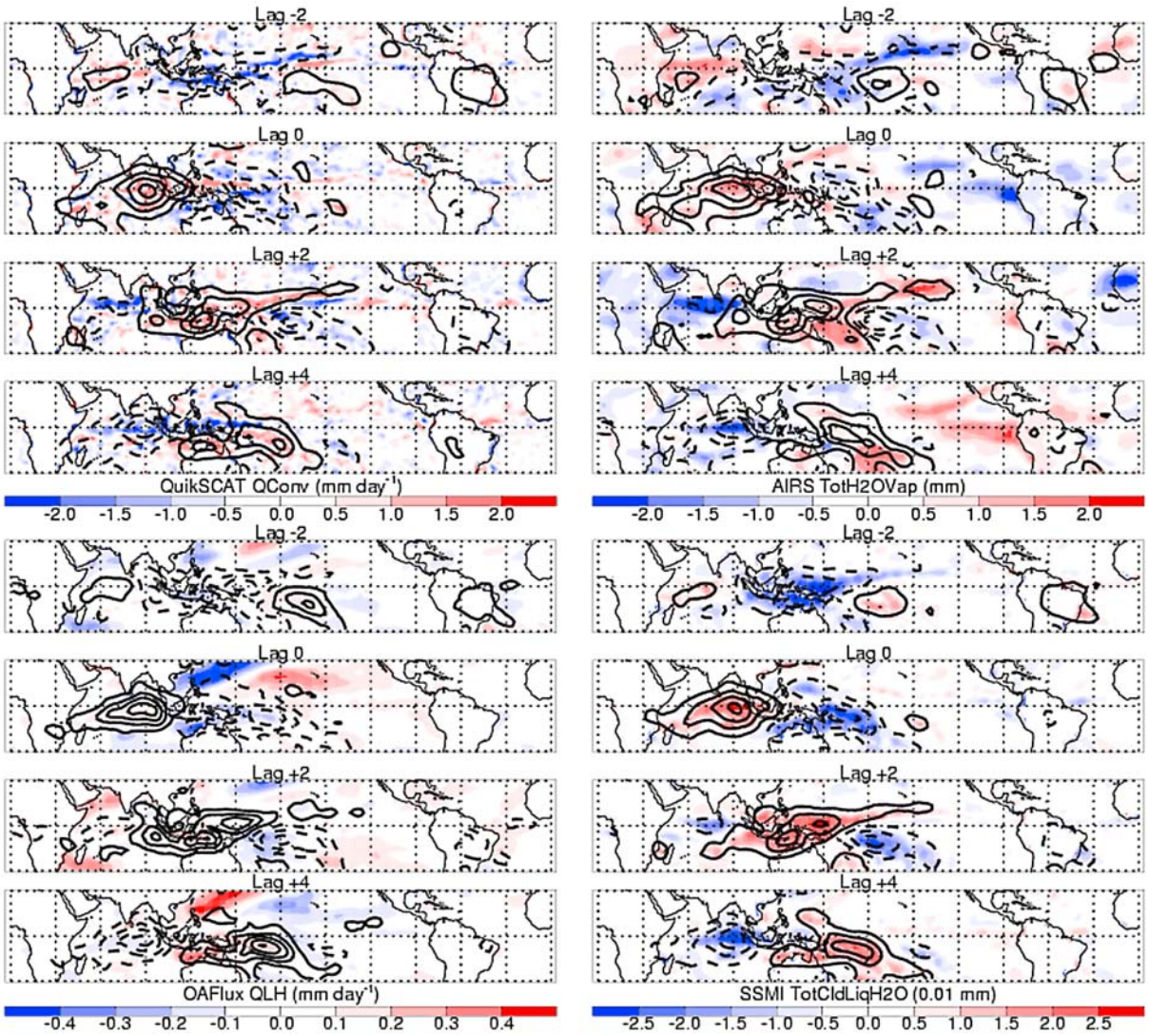

Figure 2. Color shading are maps of composite MJO anomalies of (top left) total-column moisture convergence (mm day^{-1}), (bottom left) surface evaporation (mm day^{-1}), (top right) precipitable water (mm), and (bottom right) cloud liquid water (0.01 mm). Line contours are composite CMAP rainfall anomalies (mm day^{-1}) for the period corresponding to the color shaded quantity (see Figure S1).

[10] To illustrate how well the satellite retrievals characterize the hydrological cycle of the MJO, we examine the column-integrated moisture budget relating the time rate of change of total water vapor (dW/dt) to precipitation (P), evaporation (E) and moisture convergence (C). When considering observational errors, dW/dt + P − E − C = residual. Figure 1 shows the near-equatorial meridional averages of the terms in this equation. Evident is the dominant balance between the precipitation and TCMC, with the indication of TCMC leading the precipitation slightly by about 20^{o} longitude. The values of the water vapor storage and evaporation are considerably smaller. However, it is rather disconcerting that even for this latitudinally-averaged composite, of a large-scale phenomena such as the MJO, the residual in some regions has a magnitude almost as large as the two dominant terms. For comparison, the standard deviation of the budget terms averaged over all longitudes and time lags gives 0.17, 0.10, 1.3, 1.4 and 1.3 for dW/dt, E, P, C and the residual respectively.

4. Summary

[11] The goal of this study is to provide a first ever characterization of the water cycle of the MJO using satellite-based observations. The latter now provide estimates of nearly all the sizeable and climate and/or mechanistic relevant terms. A schematic summary of the findings is in Figure 3 (bottom). The magnitudes of the anomalies are given for disturbed and suppressed phases of the MJO in the near-equatorial regions. To first order, precipitation is balanced by total column TCMC, and they are very nearly spatially and temporally in phase. The degree to which this is not true has implications for our understanding of the physical mechanisms behind the propagation and maintenance of the MJO (Tian et al., submitted manuscript, 2009).

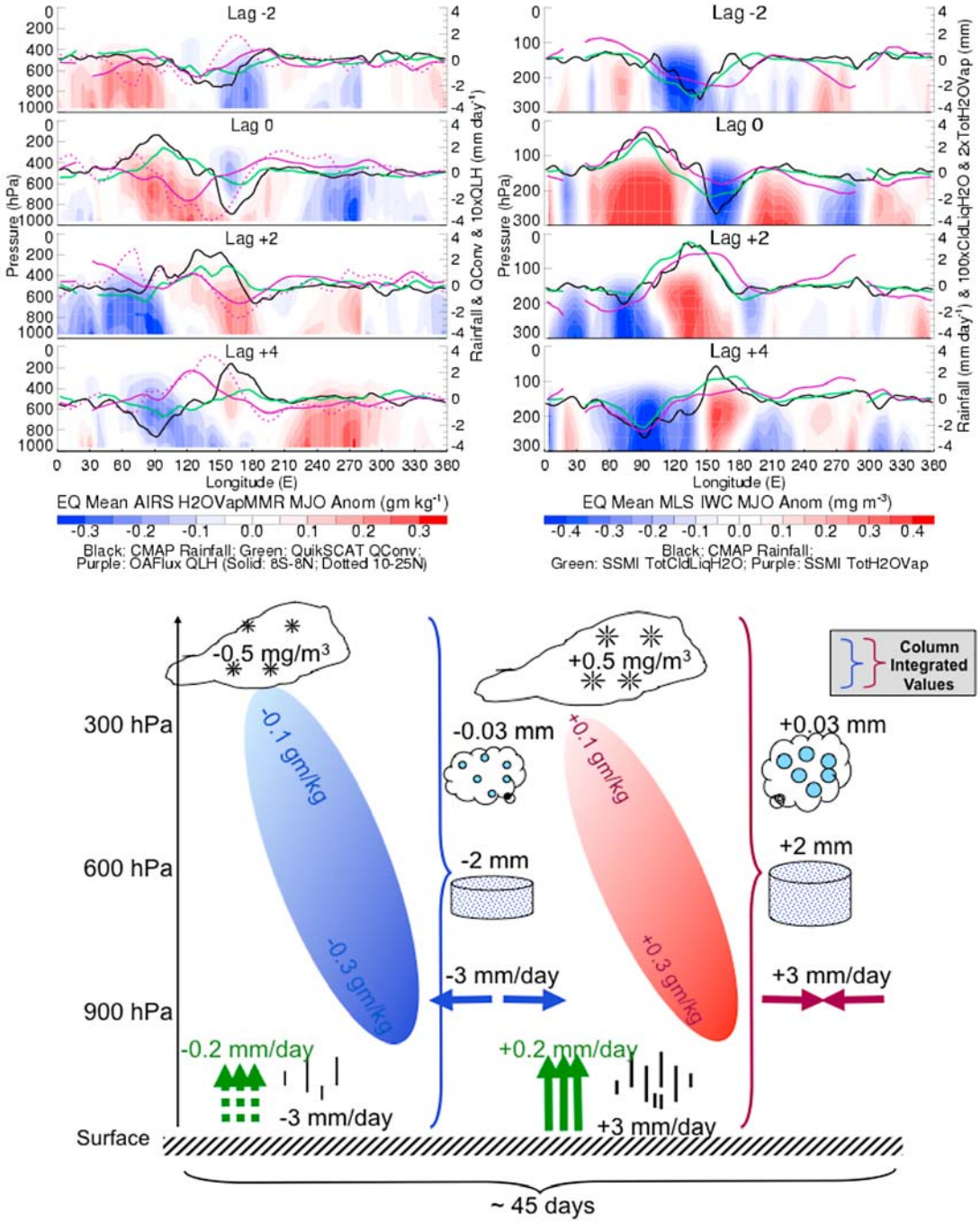

Figure 3. (top left) Pressure-longitude cross-sections of composite near-equatorial (8°S–8°N) anomalies of water vapor (gm kg^{-1}), rainfall (mm day^{-1}), moisture convergence (mm day^{-1}), surface evaporation (0.1 mm day^{-1}), and the latter using the latitude range 10–25°N. (top right) Pressure-longitude cross-sections of composite near-equatorial (8°S–8°N) anomalies of ice water content (mg m^{-3}), CMAP rainfall (mm day^{-1}), SSM/I total precipitable water (0.5 mm), and total cloud liquid water (0.01 mm). (bottom) Schematic of the hydrological cycle associated with the MJO.

The local, near-equatorial evaporation anomalies are at least a factor of 5–10 smaller than the near-equatorial precipitation anomalies, but are 2–3 times larger in geographically fixed regions that tend to lie outside the deep tropics, specifically the northwest and north central tropical Pacific and off the northwest coast of Australia. Anomalies of total column water vapor are about ±2 mm, column liquid water about 0.03 mm, and column cloud ice about 0.003 mm (the latter is a rough estimate, assuming the anomalies in Figure 3 extend over ~4000 m).

[12] While the general picture conveyed makes intuitive and physical sense, and is consistent with the components studied before (e.g., precipitation, water vapor), there are still considerable issues remaining in producing a tighter closure to the water balance – even when considering column average conditions. Notable is that the residual of

the column-average water budget has magnitudes in some locations and phases as large as the two dominate terms (i.e., precipitation and TCMC). This suggests the need for continued work in evaluation of these products, most notably TCMC. While this product has been evaluated and applied with success in a number of large-scale climatological settings [e.g., *Liu and Tang*, 2005], its application under more synoptic conditions - where the relationships between surface wind and total column transport are less systematic - needs continued testing and evaluation. This could be carried out through tests against modern reanalysis products (e.g., ERA-interim). In fact, a complete assessment of the hydrological cycle for the MJO, and a comparison to the present satellite-derived one, would be a fruitful study with one or more reanalysis products. As confidence can be attributed to the observed budget and its different terms, it can be used as a form of evaluation and validation for model simulations of the MJO. Other notable areas to investigate include understanding the pathways of moisture from the surface of the ocean to the large-scale convective regions, and the roles played by the large subtropical evaporation anomalies noted in this study, possibly with moisture tracer experiments. Finally, this study, as that of *Tian et al.* [2006], show that within the MJO life-cycle, the eastern Pacific exhibits moisture anomalies of a similar magnitude as the Indo-Pacific region. However, in the former case they seem to be limited to the lower troposphere and associated with weak or no rainfall anomalies. Determining what is responsible for these moisture anomalies and whether the rainfall products might in fact have limitations in this region (e.g., drizzle conditions) is another avenue of follow up research.

[13] **Acknowledgments.** The research described in this paper was carried out at the Jet Propulsion Laboratory, Caltech, under a contract with NASA.

References

Chahine, M. T., et al. (2006), Improving weather forecasting and providing new data on greenhouse gases, *Bull. Am. Meteorol. Soc.*, *87*(7), 911–926, doi:10.1175/BAMS-87-7-911.

Hendon, H. H., and M. L. Salby (1994), The life-cycle of the Madden-Julian Oscillation, *J. Atmos. Sci.*, *51*(15), 2225–2237, doi:10.1175/1520-0469(1994)051<2225:TLCOTM>2.0.CO;2.

Huffman, G. J., et al. (2007), The TRMM Multisatellite Precipitation Analysis (TMPA): Quasi-global, multiyear, combined-sensor precipitation estimates at fine scales, *J. Hydrometeorol.*, *8*(1), 38–55, doi:10.1175/JHM560.1.

Lau, K. M., and C. H. Sui (1997), Mechanisms of short-term sea surface temperature regulation: Observations during TOGA COARE, *J. Clim.*, *10*(3), 465–472, doi:10.1175/1520-0442(1997)010<0465:MOSTSS>2.0.CO;2.

Lau, W. K. M., and D. E. Waliser (Eds.) (2005), *Intraseasonal Variability of the Atmosphere-Ocean Climate System*, 474 pp., Springer, Heidelberg, Germany.

Lin, J. L., and B. E. Mapes (2004), Radiation budget of the tropical intraseasonal oscillation, *J. Atmos. Sci.*, *61*(16), 2050–2062, doi:10.1175/1520-0469(2004)061<2050:RBOTTI>2.0.CO;2.

Lin, J. L., et al. (2004), Stratiform precipitation, vertical heating profiles, and the Madden-Julian Oscillation, *J. Atmos. Sci.*, *61*(3), 296–309, doi:10.1175/1520-0469(2004)061<0296:SPVHPA>2.0.CO;2.

Lin, X., and R. H. Johnson (1996), Kinematic and thermodynamic characteristics of the flow over the western Pacific Warm Pool during TOGA COARE, *J. Atmos. Sci.*, *53*(5), 695–715, doi:10.1175/1520-0469(1996)053<0695:KATCOT>2.0.CO;2.

Liu, W. T., and W. Tang (2005), Estimating moisture transport over oceans using space-based observations, *J. Geophys. Res.*, *110*, D10101, doi:10.1029/2004JD005300.

Madden, R. A., and P. R. Julian (1971), Detection of a 40–50 day oscillation in the zonal wind in the tropical Pacific, *J. Atmos. Sci.*, *28*(5), 702–708, doi:10.1175/1520-0469(1971)028<0702:DOADOI>2.0.CO;2.

Mu, M., and G. J. Zhang (2006), Energetics of Madden-Julian oscillations in the National Center for Atmospheric Research Community Atmosphere Model version 3 (NCAR CAM3), *J. Geophys. Res.*, *111*, D24112, doi:10.1029/2005JD007003.

Schwartz, M. J., et al. (2008), MJO in EOS MLS cloud ice and water vapor, *Geophys. Res. Lett.*, *35*, L08812, doi:10.1029/2008GL033675.

Sperber, K. R., and D. Waliser (2008), New approaches to understanding, simulating, and forecasting the Madden-Julian Oscillation, *Bull. Am. Meteorol. Soc.*, in press.

Susskind, J., C. Barnet, J. Blaisdell, L. Iredell, F. Keita, L. Kouvaris, G. Molnar, and M. Chahine (2006), Accuracy of geophysical parameters derived from Atmospheric Infrared Sounder/Advanced Microwave Sounding Unit as a function of fractional cloud cover, *J. Geophys. Res.*, *111*, D09S17, doi:10.1029/2005JD006272.

Tian, B., et al. (2006), Vertical moist thermodynamic structure and spatial-temporal evolution of the MJO in AIRS observations, *J. Atmos. Sci.*, *63*(10), 2462–2485, doi:10.1175/JAS3782.1.

Tian, B., Y. L. Yung, D. E. Waliser, T. Tyranowski, L. Kuai, E. J. Fetzer, and F. W. Irion (2007), Intraseasonal variations of the tropical total ozone and their connection to the Madden-Julian Oscillation, *Geophys. Res. Lett.*, *34*, L08704, doi:10.1029/2007GL029451.

Tian, B., et al. (2008), Does the Madden-Julian Oscillation influence aerosol variability?, *J. Geophys. Res.*, *113*, D12215, doi:10.1029/2007JD009372.

Waliser, D. E., R. Murtugudde, and L. E. Lucas (2003), Indo-Pacific Ocean response to atmospheric intraseasonal variability: 1. Austral summer and the Madden-Julian Oscillation, *J. Geophys. Res.*, *108*(C5), 3160, doi:10.1029/2002JC001620.

Waliser, D. E., et al. (2005), Subseasonal organization of ocean chlorophyll: Prospects for prediction based on the Madden-Julian Oscillation, *Geophys. Res. Lett.*, *32*, L23602, doi:10.1029/2005GL024300.

Waliser, D. E., et al. (2009), Cloud ice: A climate model challenge with signs and expectations of progress, *J. Geophys. Res.*, *114*, D00A21, doi:10.1029/2008JD010015.

Weare, B. C., and J. S. Nasstrom (1982), Examples of extended empirical orthogonal function analyses, *Mon. Weather Rev.*, *110*(6), 481–485, doi:10.1175/1520-0493(1982)110<0481:EOEEOF>2.0.CO;2.

Weickmann, K. M., et al. (1992), The atmospheric angular-momentum cycle during the tropical Madden-Julian Oscillation, *Mon. Weather Rev.*, *120*(10), 2252–2263, doi:10.1175/1520-0493(1992)120<2252:TAAMCD>2.0.CO;2.

Wentz, F. J. (1997), A well-calibrated ocean algorithm for special sensor microwave/imager, *J. Geophys. Res.*, *102*(C4), 8703–8718, doi:10.1029/96JC01751.

Wentz, F. J., and R. W. Spencer (1998), SSM/I rain retrievals within a unified all-weather ocean algorithm, *J. Atmos. Sci.*, *55*(9), 1613–1627, doi:10.1175/1520-0469(1998)055<1613:SIRRWA>2.0.CO;2.

Wu, D. L., et al. (2006), EOS MLS cloud ice measurements and cloudy-sky radiative transfer model, *IEEE Trans. Geosci. Remote Sens.*, *44*(5), 1156–1165, doi:10.1109/TGRS.2006.869994.

Wu, D. L., et al. (2009), Comparisons of global cloud ice from MLS, CloudSat, and correlative data sets, *J. Geophys. Res.*, *114*, D00A24, doi:10.1029/2008JD009946.

Xie, P. P., and P. A. Arkin (1997), Global precipitation: A 17-year monthly analysis based on gauge observations, satellite estimates, and numerical model outputs, *Bull. Am. Meteorol. Soc.*, *78*(11), 2539–2558, doi:10.1175/1520-0477(1997)078<2539:GPAYMA>2.0.CO;2.

Xie, P. P., et al. (2003), GPCP Pentad precipitation analyses: An experimental dataset based on gauge observations and satellite estimates, *J. Clim.*, *16*(13), 2197–2214, doi:10.1175/2769.1.

Xie, X. S., et al. (2008), Spacebased estimation of moisture transport in marine atmosphere using support vector regression, *Remote Sens. Environ.*, *112*(4), 1846–1855, doi:10.1016/j.rse.2007.09.003.

Yu, L. S., and R. A. Weller (2007), Objectively analyzed air-sea heat fluxes for the global ice-free oceans (1981–2005), *Bull. Am. Meteorol. Soc.*, *88*(4), 527–539, doi:10.1175/BAMS-88-4-527.

Zhang, C. (2005), The Madden Julian Oscillation, *Rev. Geophys.*, *43*, RG2003, doi:10.1029/2004RG000158.

E. J. Fetzer, W. T. Liu, M. J. Schwartz, B. Tian, D. E. Waliser, and X. Xie, Jet Propulsion Laboratory, California Institute of Technology, MS 183-501, 4800 Oak Grove Dr., Pasadena, CA 91109, USA. (waliser@caltech.edu)